

ISO-LWS observations of rotational CO lines from C-rich objects: AFGL 2688, AFGL 618 and NGC 7027*

K. Justtanont¹, M.J. Barlow², A.G.G.M. Tielens^{3,4}, D. Hollenbach⁵, W.B. Latter⁶, X.-W. Liu², R.J. Sylvester², P. Cox⁷, N.-Q. Rieu⁸, and C.J. Skinner^{**}

¹ Stockholm Observatory, 133 36 Saltsjöbaden, Sweden

² Department of Physics and Astronomy, University College London, Gower Street, London, WC1E 6BT, UK

³ Kapteyn Institute, P.O. Box 800, 9700 AV Groningen, The Netherlands

⁴ SRON-Groningen, P.O. Box 800, 9700 AV Groningen, The Netherlands

⁵ NASA Ames Research Center, MS 245-3, Moffett Field, CA 94035, USA

⁶ SIRT Science Center/IPAC, Caltech, MS 314-6, Pasadena, CA 91125, USA

⁷ IAS, Bat. 120, Université de Paris XI, 91405 Orsay, France

⁸ Observatoire de Paris, 61 avenue de l'Observatoire, 75014 Paris, France

Received 25 February 2000 / Accepted 23 June 2000

Abstract. We present ISO-LWS full scan observations of CO rotational emission lines (J=14-13 up to J=37-36) from two C-rich post-AGB objects, AFGL 2688; AFGL 618, and one C-rich PN, NGC 7027. The presence of high rotational lines cannot be explained by a spherical, constant velocity wind during the previous AGB phase, but indicates a layer of warm, dense gas with a substantial beam filling factor ($\Omega > 10^{-10}$ sr). By simple optically thin calculations, we estimate the total mass of gas cooled through CO rotational lines to be typically $\sim 0.1 M_{\odot}$.

We also consider the physical processes responsible for heating and cooling the warm gas in these objects. Energy sources for the gas could include FUV photons, resulting in a PhotoDissociation Region (PDR), as well as shocks driven by the interacting winds during this evolutionary phase. We have calculated detailed models for the heating and cooling in C-rich PDRs and shocks in order to explain the CO spectra observed. In both models, the gas is cooled radiatively by molecular rotational lines as well as by atomic fine structure lines. Both models can produce warm gas of >500 K at a density of $10^6 - 10^7 \text{ cm}^{-3}$.

We conclude that the source of heating for the young PN, NGC 7027, is FUV photons from the central star. For the least evolved post-AGB star, AFGL 2688, the effective temperature is too cool to produce many FUV photons to heat the gas. However, there is evidence of a fast wind developing and hence the most likely heating mechanism for the envelope is shocks. For AFGL 618, the central star is hot enough to provide copious amounts of FUV photons but fast outflows have also been observed and both processes may be operational. However, in

view of [O I] $63 \mu\text{m}$ high resolution observations, the heating mechanism is more likely to be a PDR.

Key words: stars: circumstellar matter – stars: evolution – stars: individual: NGC 7027, AFGL 618, AFGL 2688 – stars: late-type – stars: mass-loss – infrared: stars

1. Introduction

Mass loss from a star at the end of the Asymptotic Giant Branch (AGB) is thought to be in the form of a superwind. At this stage, the star experiences a sudden increase in its mass loss rate by up to an order of magnitude. This explanation, accompanied by modelling, was used by Justtanont et al. (1996) to interpret observations of the extreme OH/IR star, OH26.5+0.6. The mass loss rates drop by several orders of magnitude once the star evolves off the AGB. The effective temperature of the star rises as it moves across the HR diagram and becomes a Planetary Nebula (PN) when its surrounding shell is ionized ($T_{\text{eff}} \sim 3 \cdot 10^4$ K). The enhanced mass loss has been seen in the archetype C-star, IRC+10 216 (Mauron & Huggins 1999) and in the HST images of AFGL 2688 as multiple rings around the central star (Sahai et al., 1998a, 1998b). The latter has evolved off the AGB.

Three high rotational transitions of CO have previously been observed by Justtanont et al. (1997), using the Kuiper Airborne Observatory (KAO) from AFGL 2688, AFGL 618 and NGC 7027. These observations revealed the presence of a warm dense molecular layer. This molecular gas has to be heated either through shocks due to the interaction of the fast and the AGB winds or through FUV photons from the central star or both. Liu et al. (1996) and Cox et al. (1996) presented preliminary ISO LWS results of NGC 7027 and AFGL 2688, respectively. Both discussed the need for a warm molecular layer in order to explain the observations. In this paper, we explore the heating

Send offprint requests to: K. Justtanont (kay@astro.su.se)

* Based on observations with ISO, an ESA project with instruments funded by ESA Member States (especially the PI countries: France, Germany, the Netherlands and the United Kingdom) with the participation of ISAS and NASA.

** Deceased

and cooling mechanisms in these objects and in AFGL 618 in more detail.

It is known that FUV photons create a photodissociation region (PDR) around hot stars. The gas is believed to be heated by the photoelectric effect on small grains (Tielens & Hollenbach 1985, hereafter TH85) and/or polycyclic aromatic hydrocarbons (Bakes & Tielens 1994). It is cooled mainly via atomic fine structure lines of [O I] 63 and 146 μm and [C II] 158 μm , as well as molecular rotational lines of CO. For cooler stars, UV photons are not very effective in the heating (Spaans et al. 1994). However, post-AGB stars have been observed to develop a fast wind which leads to shocks when this wind collides with the slower moving, previously ejected, AGB wind. The shock-heated gas can cool via [O I] lines (if atomic oxygen is present) and molecular rotational lines. There are two different types of shocks: C- and J-shocks. The former continuous shock is characterized by relatively slow shock velocities; molecules behind the shock fronts are not dissociated; and atoms remain neutral. Magnetic fields play an important role in C-shocks. Jump shocks, or J-shocks, show a discontinuity between the pre- and post-shock material. The shock velocity is relatively fast and molecules are generally dissociated and atomic species can be ionized. J-shocks have smaller warm columns of neutral gas than PDRs, so they require higher densities to produce the same [O I] intensity. Because higher density gas produces higher [O I]/[CII] ratios (TH85), J-shocks have a higher ratio of [O I]/[CII] than PDRs with the same [O I] intensity (Hollenbach & McKee 1989, hereafter HM89).

In Sect. 2, we present observations of rotational CO lines observed using the Long Wavelength Spectrometer (LWS, Clegg et al. 1996; Swinyard et al., 1996) aboard the Infrared Space Observatory (ISO, Kessler et al. 1996), which gives a full coverage between 43-197 μm . The implications of a simple analysis of the data are presented in Sects. 3 and 4. Various possible heating mechanisms are discussed in Sect. 5 and results from individual objects are compared to model calculations in Sect. 6.

2. Observations

The spectra of the C-rich post-AGB stars, AFGL 2688 and AFGL 618, along with that of the C-rich PN NGC 7027 were taken with ISO-LWS in full grating mode with an average resolving power of ~ 200 . NGC 7027 was observed with oversamplings ranging from 1/4.5 to 1/15 of a resolution element (see Liu et al. 1997 for full details), with a total integration time of 23 930 sec. AFGL 2688 was also observed with a non-standard observation (COIF) with an oversampling rate of 1/15 and a total integration time of 15 669 sec while AFGL 618 was observed with a standard LWS01 AOT with an oversampling rate of 1/4 of a resolution element and a total integration time of 3 641 sec. The fluxes were calibrated with respect to Uranus (Swinyard et al. 1996). The ten subspectra obtained as part of each spectrum have overlaps and hence were adjusted slightly in order to obtain the final smooth overall spectrum for each object. All spectra were reduced with the OLP7 LWS pipeline.

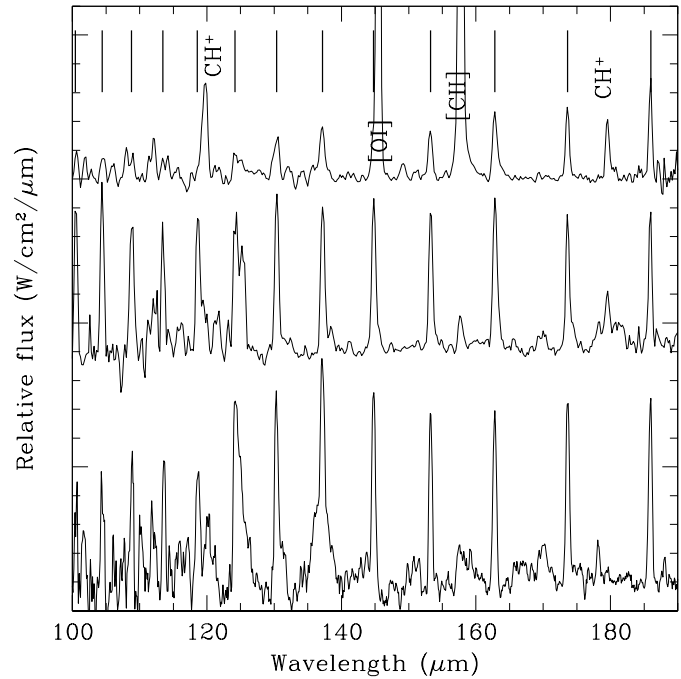


Fig. 1. Continuum subtracted spectra of NGC 7027 (top), AFGL 618 (middle) and AFGL 2688 (bottom) along with CO rotational line positions from $J=14-13$ to $J=26-25$ marked as vertical bars. Other known emission lines are also indicated.

The objects span a number of evolutionary phases, from having recently left the AGB (AFGL 2688); to a more evolved object with a hotter central star (AFGL 618); to a young planetary nebula with a very hot central star (NGC 7027). There is, in general, an increasing trend of a faster wind and more FUV photons as a star evolves to become a PN. Fig. 1 shows the continuum subtracted spectra of the stars in our sample, with vertical bars marking the wavelengths of CO rotational transitions. Also seen, but not indicated, are HCN emission bands which form part of emission seen in AFGL 2688 (see e.g., Cernicharo et al. 1996). We fitted Gaussians to all the CO lines detected and the estimated line fluxes are listed in Table 1. The estimated errors reflect the uncertainty in defining the local continuum for each line and hence are minimum errors. Our estimated line fluxes of NGC 7027 agree well with those of Liu et al. (1996), but our line fluxes for AFGL 2688 differ from those of Cox et al. (1996). The latter reflect the difficulty in determining the local continuum baseline due to emission plateau from HCN and, as yet, unidentified molecular transitions. We detected CO lines up to $J=27-26$ from both AFGL 2688 and NGC 7027 as the higher J lines are indistinguishable from the noise in the SW part of the spectrum. For AFGL 618, we detect lines up to the $J=37-36$ line before the noise prevents the possible identification of higher J lines.

It should be noted that the earlier observations done with the KAO (Justtanont et al. 1997) yielded higher fluxes than those from LWS, by up to a factor of two in some cases (see Figs 6-8). Comparisons of the LWS continuum flux levels with preexisting

Table 1. Observed CO line fluxes

transition	λ (μm)	Line flux ($\times 10^{-19} \text{ W cm}^{-2}$)		
		AFGL 2688	AFGL 618	NGC 7027
J=14-13	186.00	4.8 \pm 0.2	3.1 \pm 0.9	2.0 \pm 0.1
J=15-14	173.63	4.7 \pm 0.2	3.3 \pm 0.6	1.7 \pm 0.1
J=16-15	162.81	4.5 \pm 0.3	4.2 \pm 0.7	1.6 \pm 0.1
J=17-16	153.27	4.0 \pm 0.3	3.6 \pm 0.4	1.1 \pm 0.1
J=18-17	144.78	5.0 \pm 0.7	3.8 \pm 1.2	1.1 \pm 0.2
J=19-18	137.20	5.8 \pm 0.5	3.8 \pm 0.7	1.2 \pm 0.1
J=20-19	130.37	5.0 \pm 0.8	4.0 \pm 0.9	1.0 \pm 0.1
J=21-20	124.19	4.8 \pm 0.9	3.5 \pm 1.0	0.7 \pm 0.1
J=22-21	118.58	3.6 \pm 0.6	3.6 \pm 0.7	0.3 \pm 0.1
J=23-22	113.46	2.9 \pm 0.5	2.9 \pm 0.5	0.5 \pm 0.1
J=24-23	108.76	3.1 \pm 0.5	3.6 \pm 0.5	0.7 \pm 0.1
J=25-24	104.44	2.6 \pm 0.6	4.6 \pm 0.4	0.5 \pm 0.1
J=26-25	100.46	2.3 \pm 0.7	3.2 \pm 0.4	0.7 \pm 0.1
J=27-26	96.77	1.8 \pm 0.8	4.1 \pm 1.0	0.5 \pm 0.1
J=28-27	93.35	-	2.8 \pm 1.0	-
J=29-28	90.16	-	3.8 \pm 2.0	-
J=30-29	87.19	-	2.4 \pm 1.4	-
J=31-30	84.41	-	1.1 \pm 1.3	-
J=32-31	81.81	-	6.6 \pm 2.6	-
J=33-32	79.36	-	1.9 \pm 1.3	-
J=34-33	77.06	-	2.6 \pm 1.4	-
J=35-34	74.89	-	2.3 \pm 1.3	-
J=36-35	72.84	-	3.2 \pm 1.3	-
J=37-36	70.91	-	3.1 \pm 2.8	-

IRAS and KAO photometry of these objects indicate excellent agreement however.

3. CO rotational lines

Since we measure a series of rotational CO line fluxes, we present them as a rotation diagram (Fig. 2). If we assume LTE, we can derive the temperature of the gas, T_x .

Assuming that the CO emission is optically thin, the flux F_{ji} for transition j to i is given by

$$F_{ji} = N_0 \frac{\exp(-E_j/kT_x)}{\Phi(T_x)} \frac{A_{ji} h \nu_{ji} g_j}{4\pi d^2} \quad (1)$$

where d is the distance to the source, A_{ji} is the Einstein spontaneous transition probability, ν_{ji} is the frequency of the transition, g_j and E_j are the statistical weight and energy above the ground state of the upper level j , N_0 is the total number of molecules and $\Phi(T_x)$ is the partition function. By rearranging the above equation, we get

$$\begin{aligned} E_j/kT_x &= \ln(N_0/\Phi(T_x)d^2) - \ln(4\pi F_{ji}/A_{ji}h\nu_{ji}g_j) \\ &\equiv \ln(N_0/\Phi(T_x)d^2) - Y_j. \end{aligned} \quad (2)$$

The derived excitation temperatures, i.e., the slopes of the best fits for these objects fall into a range of 300-600 K (Table 2). The temperature for AFGL 618 is slightly higher than for the other two objects as exemplified by the higher rotational transitions observed. The fact that we observe these emission lines points to high density gas. Indeed, the approximate linear behaviour

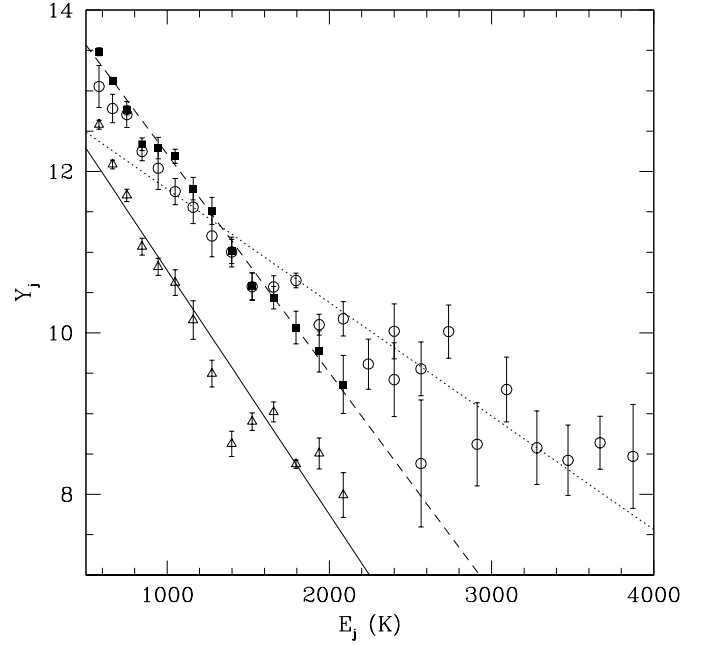


Fig. 2. Rotation diagram of our sampled stars: triangles-NGC 7027; circles-AFGL 618; filled squares-AFGL 2688. The straight lines are the best fits from which the rotation excitation temperatures in Table 2 are derived (see Eq. 2).

in the rotation diagram indicates thermalization of levels up to $J \simeq 27$. This requires fairly high density ($n \gtrsim 10^5 \text{ cm}^{-3}$) and warm ($T \gtrsim 300 \text{ K}$) gas. Although the stars are in different evolutionary stages, the regions emitting the CO lines seem to have very similar properties.

Using the rotation diagram and the calculated rotation temperature, we can calculate the total number of emitting molecules, assuming that the partition function, $\Phi(T_x)$ can be approximated as $(T_x/2.77)\text{K}$ (McKee et al. 1982). Since the distance of AFGL 2688 is not well known, we adopt a distance of 1 kpc for this object. For AFGL 618 and NGC 7027, we have taken distances of 1.8 kpc (Schmidt & Cohen 1981) and 790 pc (Pottasch 1996), respectively. We are able to reasonably fit each dataset with a single temperature. For AFGL 618, the fit to the higher-J lines is not very good. This could be due either to observational uncertainty of the line fluxes or to an intrinsic property of the object, e.g., higher-J lines originate from hotter gas, or it could imply that at high-J levels, CO populations are no longer in LTE. The results which are summarized in Table 2 show appreciable masses of CO gas involved in cooling the envelopes. These translate into total masses of gas being cooled by CO of the order of $0.1 M_\odot$, assuming a CO/H abundance ratio of 6×10^{-4} .

4. Optically thin slab model

As a first approximation to modelling the CO line emission, we assume that the high-J CO lines are optically thin. Following TH85, we solve the equation of statistical equilibrium at a spe-

Table 2. Derived parameters from the rotation diagrams (see text for details).

	T_x (K)	D (pc)	N_{CO} (molecules)	M_{CO} (M_\odot)	M_H (M_\odot)
AFGL 2688	380 ± 30	1000	$3.6E+51$	$8.5E-5$	0.14
AFGL 618	700 ± 90	1800	$4.4E+51$	$1.0E-4$	0.17
NGC 7027	350 ± 15	790	$6.7E+50$	$1.6E-5$	0.03

Table 3. Estimated temperature and density for best fit models assuming optically thin CO emission (Fig. 3). The numbers in parenthesis are alternative model fits.

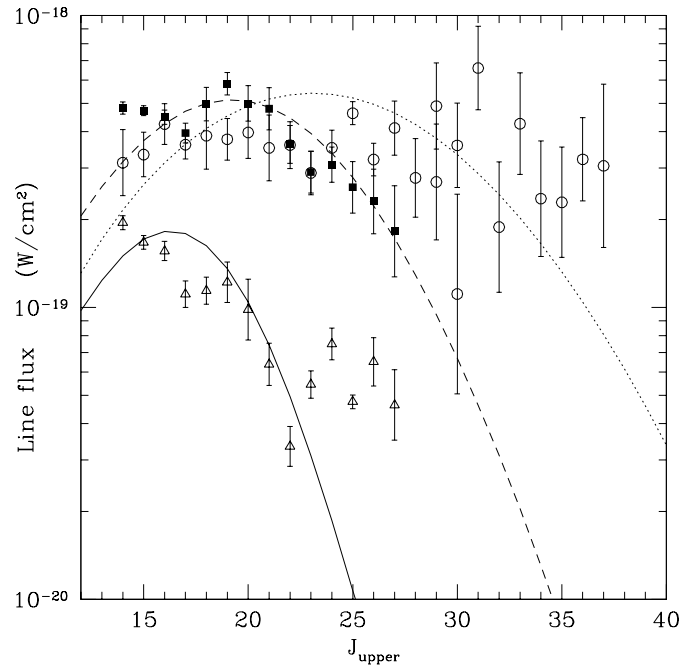
	T_g (K)	n (cm^{-3})	T_d (K)	τ_d
AFGL 2688	380 (2 000)	$5 \cdot 10^7$ ($2 \cdot 10^5$)	380 (1 000)	0.5 (0.5)
AFGL 618	700 (2 000)	$5 \cdot 10^7$ ($5 \cdot 10^5$)	700 (1 000)	0.5 (0.5)
NGC 7027	350 (1 000)	10^6 (10^5)	350 (500)	0.5 (1.0)

cific temperature and density. The cooling rate by a transition from level i to j is given by

$$\Lambda_{ij} = n_i A_{ij} E_{ij} (1 - P_{ij}/S_{ij}) \quad (3)$$

where S_{ij} is the source function and P_{ij} takes into account the 2.7 K background radiation and that due to dust. The dust background radiation is given by a modified black body with a λ^{-1} emissivity, an optical depth, τ_d at $100 \mu\text{m}$, and a dust temperature, T_d . We approximate the collisional (de)excitation using the formulation by de Jong et al. (1975). Fig. 3 shows the fits to the observed fluxes, assuming optically thin emission from a slab. The peak in the line intensity distribution, J_{max} , is very dependent on the input gas density, n , while the maximum flux depends on a combination of the gas and dust temperature, the dust optical depth and the gas column density. Both the gas and dust temperatures have a similar effect in raising the fluxes of high transition lines, making the slope of the fit shallower for $J > J_{\text{max}}$, but with the former having a much greater effect on the slope than the latter. Increasing the density results in J_{max} shifting towards higher J . However, different combinations of these parameters can produce similar fits so there is no unique solution. For the range of temperatures investigated (up to 2 000 K), the density ranges from $10^5 - 10^7 \text{ cm}^{-3}$.

The parameters used to fit each dataset are listed in Table 3. We are able to fit most lines in AFGL 2688, AFGL 618 and NGC 7027 with a single temperature and density. These simple fits indicate densities of $\sim 10^6 - 5 \cdot 10^7 \text{ cm}^{-3}$ if we assume temperatures are the same as those derived from the rotation diagrams (Table 2). Note that the high density is above the critical density required for $J=19-18$ transition hence the gas is fully in LTE. Below this density, the gas drops out of LTE hence the gas temperature will not necessarily be the same as the excitation temperature. As we noted previously, the parameters used are not unique to the fit. A reasonably good fit can be obtained with a high temperature and somewhat lower density. The LTE assumption breaks down and the gas is subthermally excited hence the gas temperature is much higher than the excitation temperature. Even though the density is low but the calculation takes into account the excitation hence at high temperature, the high

**Fig. 3.** Optically thin slab models used to fit the observed CO line fluxes. The solid line is a model with $T=350 \text{ K}$ and $n = 10^6 \text{ cm}^{-3}$ while $T=380 \text{ K}$ and $n = 5 \cdot 10^7 \text{ cm}^{-3}$ for the dashed line and $T=700 \text{ K}$ and $n = 5 \cdot 10^7 \text{ cm}^{-3}$ for the dotted line. We use the same symbols for the sources as in Fig. 2.

J lines are excited to give results close to observed line fluxes. These alternative models are also listed in Table 3 in parentheses. In the low temperature case, the density is high enough that the high J levels are substantially populated in order to give the observed line fluxes. In contrast, the high temperature case requires much lower density but the kinetic temperature is high enough to excite molecules to high J levels. By simply fitting the distribution of line fluxes over J levels, we cannot distinguish between these two competing cases, although the rotation diagram favours the low temperature and high density case. Our high temperature results for NGC 7027 agree with those obtained by Liu et al. (1996) who also calculated an optically thin model for these CO lines.

We emphasize here that the above calculations do not take into account the physics of the gas, i.e., heating and cooling mechanisms. In order to explain the observed line fluxes, we have to explain how the gas is heated enough in order to emit these high transitions. Photons from these lines then escape from the surrounding medium, cooling the gas. We will briefly touch upon radiative cooling via atomic fine structure lines, which also contributes significantly. Their fluxes can also be used, in conjunction with the CO rotational lines, to constrain the inputs to the calculations. In the next section, we discuss more physical models for the emission from these regions.

5. Heating mechanisms

It has been shown that the high level CO lines observed in post-AGB objects and PNe cannot result from the emission of an

AGB wind radiating its thermal energy content away. Indeed, a model with a constant wind predicts CO high rotational line fluxes which are well below the observations (Cox et al. 1996; Justtanont et al. 1997). Therefore, other mechanism(s) must be sought to explain how the gas can be heated to a high temperature in order for these CO lines to be seen. In the previous section, a simple, first-approach analysis of our data, indicating the presence of a layer of warm, dense gas around the stars, without considering the physical cause for such a layer. Here, we discuss the probable mechanisms which heat the gas and excite the high CO rotational lines observed in the LWS data.

Hot central stars like the nuclei of PNe produce FUV photons which are efficient in ionizing atoms, dissociating molecules and heating the dust. This leads to a PDR which can heat up the surrounding gas. However, for cooler stars, this is not the case. The heating is mainly due to a newly developed fast wind which sweeps up materials in the outflow creating a shocked region and heating the gas in the process. Both mechanisms have been used to explain the observed atomic fine structure lines (e.g., [O I] and [C II]) in various environments, ranging from HII regions around young stars to PNe and the galactic centre (e.g., Burton et al. 1990; Cohen et al., 1988; Draine & McKee 1993; Hollenbach & Tielens 1997; Lester et al., 1981).

5.1. Shock model

In this section, we exclusively discuss the J-shock models since we see the [C II] 158 μm line in our sample objects, which indicates the shock, if present, is dissociative and no appreciable magnetic field is expected in these circumstellar environments. The basic calculation of heating and cooling due to a J-shock is described by HM89. We present models with low shock velocities (20 and 30 km s^{-1}) and different preshock densities (10^6 - 10^7 cm^{-3}) for a C/O ratio of 2 (i.e., O/H = $3.1 \cdot 10^{-4}$ and C/H = $6.2 \cdot 10^{-4}$) and 4.8 (i.e., C/H = $1.5 \cdot 10^{-3}$). Although the chemistry is not fully adapted for a C-rich case, we assume here that the chemistry of the molecular layer is not greatly affected by the lack of C-reactions and that the CO line intensities scale with the abundance of O since CO is thought to be one of the first molecules to form after the gas is photodissociated by shock waves. Plots of different models are presented in Fig. 4, which shows the CO intensities as a function of preshock density, n_0 , and velocity, v_s .

For the cases with C/O=2, increasing the shock velocity from 20 to 30 km s^{-1} while holding the preshock density the same reduces the CO intensity by almost a factor of two for high-J lines. A 20 km s^{-1} shock does not dissociate much of CO molecules while a 30 km s^{-1} shock does. A further increase in shock velocity above 30 km s^{-1} will increase the CO line intensities and produce a general shift of the emission curve to higher J (c.f., HM89), as CO reforms in the warm postshock gas. An increase in density by a factor of ten, while keeping all other parameters the same, results in an increase in the CO intensity by a factor of ~ 1.5 . Although this reflects the larger total column of warm CO molecules, the CO emission at such

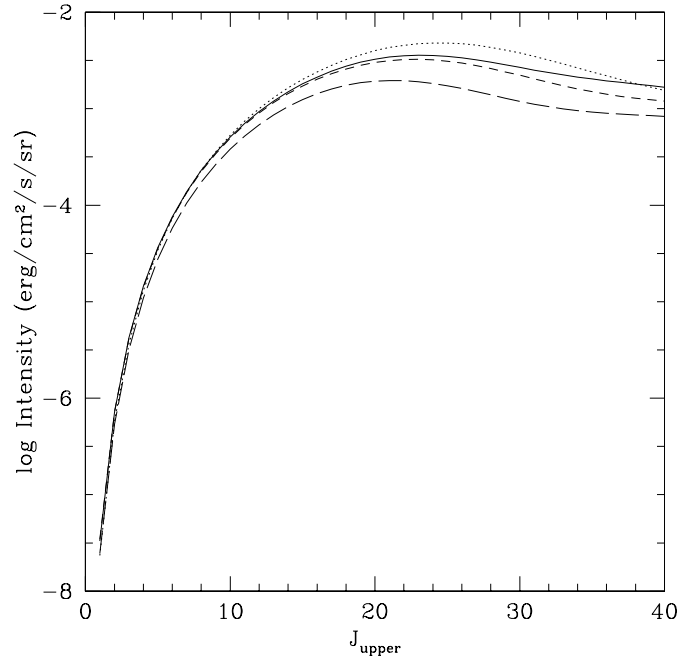


Fig. 4. CO line intensities from different shock models. Solid line: $n_0 = 10^6 \text{ cm}^{-3}$; $v_s = 20 \text{ km s}^{-1}$; C/O=2. Short dashed line: $n_0 = 10^7 \text{ cm}^{-3}$; $v_s = 30 \text{ km s}^{-1}$; C/O=2. Long dashed line: $n_0 = 10^6 \text{ cm}^{-3}$; $v_s = 30 \text{ km s}^{-1}$; C/O=2. Dotted line: $n_0 = 10^6 \text{ cm}^{-3}$; $v_s = 20 \text{ km s}^{-1}$; C/O=4.8.

high preshock densities comes from the optically thick region since the postshock density can increase by 10-100 times the preshock density. The CO line intensity increases only slightly with increasing C/O ratio since the CO abundance is, of course, limited by the O/H abundance and because the lines are optically thick.

5.2. C-rich PDR model

Based on the work by TH85, models for PDRs have been developed (Latter & Tielens 2000, in prep.) which take into account the C-rich chemistry in the reaction network. The code includes a total of 94 atomic and molecular species connected by 1270 reactions. It also includes the effects of X-ray ionizations and heating. We adopted this latest model in order to describe the LWS observations. At present, we calculate CO line intensities up to the J=50 level.

Similar to the shock case, we have constructed a grid of models with different values for the density and incident FUV radiation fields. We considered models with two different incident FUV fields, G_0 (in units of the average interstellar flux of $1.6 \times 10^{-3} \text{ erg cm}^{-2} \text{ s}^{-1}$, Habing 1968): $5 \cdot 10^5$ and 10^7 . For each set, we have calculated CO intensities for densities of 10^5 , 10^6 and 10^7 cm^{-3} . We have adopted O/H= 6.2×10^{-4} and C/H= 1.9×10^{-3} , giving a maximum CO/H abundance of 6.2×10^{-4} .

As can be seen in Fig. 5, an increase in either G_0 or density, n , results in an increase in the line intensity. An important contribution to the heating comes from collisional deexcitation

of FUV-pumped vibrationally excited H_2 , and the heating rate is somewhat sensitive to G_0 and n . An increased G_0 leads to a higher heating rate of the gas and therefore to a higher gas temperature. As a result, CO line intensities increase and the maximum of the curves in Fig. 5 shifts towards higher J . Increasing density also leads to an increase in heating and higher gas temperatures. Furthermore, the increased density increases the excitation of subthermally excited lines. The increase in the CO line intensities with increasing density is therefore more pronounced than for an increase in G_0 .

As a test, we have also calculated an O-rich model with $C/O=0.5$ for the highest values of density and G_0 , with C/H and O/H abundances of $6.2 \cdot 10^{-4}$ and $1.2 \cdot 10^{-3}$, respectively. The resulting CO line intensity is a factor of 1.3 lower than the corresponding model with other input parameters held the same. The small decrease is due to the fact that the CO abundance remains more or less the same in both cases ($6.2 \cdot 10^{-4}$, i.e., it traces the abundance of the less abundant species), but the total column density of CO decreases by a small amount. As we have shown in our previous work (Justtanont et al. 1997), the CO cooling scales with the input CO abundance. However, the changes in the resulting fine structure lines of [O I] and [C II] scale with the relative C and O abundances left over after the formation of CO, i.e., with $C/O=0.5$, the cooling due to [O I] is 2.5 times that for $C/O=3.0$ and the cooling due to [C II] in the former case is half that of the latter.

6. Discussion

In this section, we discuss the application of the shock and PDR models to our data. In order to compare the observed fluxes to the model calculations, we have to convert fluxes to intensities by assuming a source size (Ω). For this we use the observed size of the NIR H_2 emission because it is thought to arise from the H_2 formation region either at the surface of a PDR or just behind a shock front. This gives a lower limit to the source size, however.

6.1. AFGL 2688

This object has recently left the AGB and the central star is still relatively cool, with an F5 Ia spectral type (Crampton et al. 1975). Hence, the central star is too cool to provide copious amounts of FUV photons to heat the gas. Sub-mm CO observations of this object (Young et al. 1992) show that the outflow is complex and different velocity components exist, ranging from a relatively slow wind of 20 km s^{-1} (AGB wind) to a fast wind of 100 km s^{-1} . Recently, Cox et al. (2000) reported high resolution CO observations which showed multiple outflows with different velocities ($v \leq 30 \text{ km s}^{-1}$) which are recently ejected from the star. The density inferred from a combination of such observations and from HST observations (Sahai et al. 1998b) is very high, suggesting that the star has lost a large amount of mass in a short period of time ($\dot{M} \sim 10^{-4} M_{\odot} \text{ yr}^{-1}$), known as a superwind. Since there is a difference in the velocity of the outflows, this naturally results in shocks propagating through the

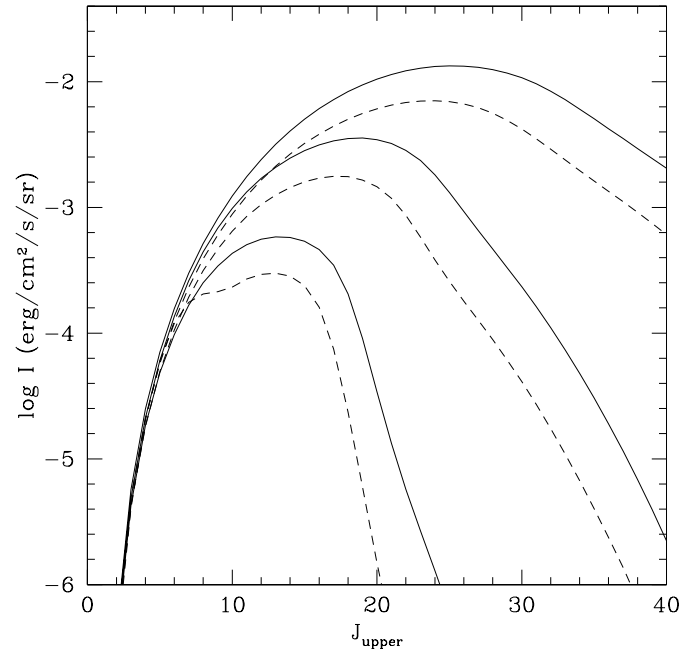


Fig. 5. CO line intensities from different PDR models. The dashed lines are for $G_0 = 5 \cdot 10^5$ and the solid lines are for $G_0 = 10^7$. Each set has three lines with densities of 10^5 , 10^6 and 10^7 cm^{-3} showing increasing CO line intensities.

medium, which are a source of heating. Hora & Latter (1994) and Hora et al. (1999) also confirmed this conclusion from their study of H_2 emission lines in the near-IR.

We can compare the observations with the grid of shock models in Sect. 5.1 (see also Fig. 4). Even though the actual CO/H ratio may be higher than our model runs, the change in the CO cooling will be minimal since the lines in our models are optically thick. From H_2 images presented by Cox et al. (1997); Latter et al. (1993); Skinner et al. (1997) and Sahai et al. (1998b), the total solid angle of all four clumps is about $2 \cdot 10^{-9} \text{ sr}$. The models give a reasonable fit to the observations within the preshock density upper limit of $10^6 - 10^7 \text{ cm}^{-3}$ and a shock velocity of $20\text{-}30 \text{ km s}^{-1}$ (Fig 6), but possibly points towards a slightly lower density in view of the fall off of the high- J line intensities. This, at first, seems to contradict the much higher density inferred from the optically thin LTE calculation (Sect. 4). However, the post-shock density can be much higher than the preshock density where the CO emission is thought to occur downstream from the shock front. Although there is evidence from low- J CO observations of higher velocity gas (Young et al. 1992), high velocity shocks cannot account for the CO line fluxes observed with the LWS. High velocity shocks ($v_s \gtrsim 100 \text{ km s}^{-1}$) are highly dissociative and predict peak CO intensity at $J=23$, while the flux should level off towards higher J (HM89). From our observations, the peak emission is closer to $J=19$, with relatively bright lower J lines and a decline beyond $J>20$. A high shock velocity model also predicts a relatively bright [O I] $63 \mu\text{m}$ line, which is not seen in the spectrum (see below). The best models to describe such an effect are those with high density and low shock velocity (Fig. 6).

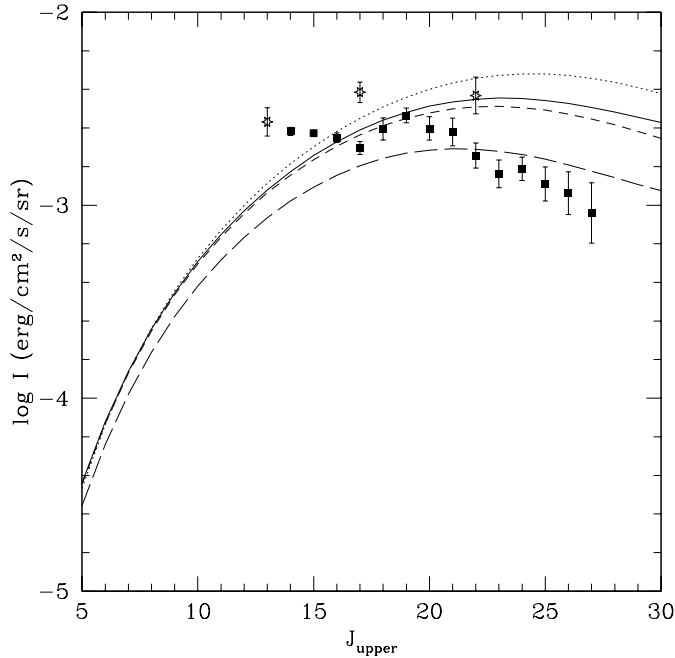


Fig. 6. Comparison between shock models and the observed LWS (squares) and KAO (stars) CO line intensities for AFGL 2688. See Fig. 4 for the key to the different models. The assumed source size is $2 \cdot 10^{-9}$ sr.

Cox et al. (1996) reported a good fit to the LWS CO line fluxes using a model with a density of 10^7 cm^{-3} , a shock velocity of 60 km s^{-1} and a gas temperature of 400 K. We have also derived a high density of $10^6 - 10^7 \text{ cm}^{-3}$. Cox et al. stated that the spectrum of AFGL 2688 shows no evidence of [O I] atomic fine structure lines, while the [C II] line may be present on a plateau of an unidentified feature. We can confirm the lack of the [O I] 63 and $146 \mu\text{m}$ and [C II] $158 \mu\text{m}$ lines from our spectrum (Fig. 1). This can be used to constrain an upper limit to the shock velocity in our models. The 20 km s^{-1} shock model predicts line fluxes for the [O I] $63 \mu\text{m}$ and [C II] $158 \mu\text{m}$ lines of $2 \cdot 10^{-23}$ and $5 \cdot 10^{-25} \text{ W cm}^{-2}$, assuming $\Omega = 2 \cdot 10^{-9}$ sr. These predicted values are consistent with their non-detection by the LWS in its grating scan mode. In contrast, the 30 km s^{-1} shock model predicts brighter [O I] lines (e.g., the [O I] $63 \mu\text{m}$ line is expected to be $\sim 10^{-18} \text{ W cm}^{-2}$) for both preshock densities of 10^6 and 10^7 cm^{-3} . Essentially, in contrast to the 20 km s^{-1} shocks, a velocity of 30 km s^{-1} is able to ionize some carbon giving rise to brighter [C II] $158 \mu\text{m}$ emission also.

6.2. AFGL 618

This object has also been intensely studied in the IR and sub-mm since it is a bright, post-AGB star on the verge of becoming a PN. The central star has a spectral type B0, with a temperature of $3 \cdot 10^4 \text{ K}$ (Schmidt & Cohen 1981). The H and K band images reveal a bipolar extension in the E-W direction extending about $3''$ (Latter et al. 1992). Hence, the source size in H_2 emission is only $2 \cdot 10^{-10}$ sr. Although the central star produces enough FUV photons to heat and ionize the nebula surrounding it, a fast wind

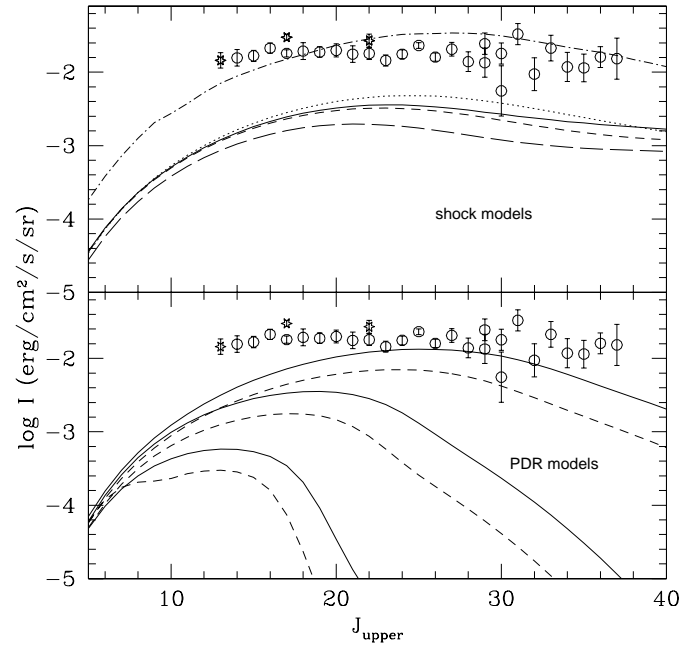


Fig. 7. Comparison between LWS (circles) and KAO (stars) CO line intensities for AFGL 618 and the PDR (lower) and shock (upper) models. The dot-dashed line is a scaled shock model for $n_0 = 10^6 \text{ cm}^{-3}$ and $v_s = 150 \text{ km s}^{-1}$, from HM89. The assumed source size is $2 \cdot 10^{-10}$ sr.

is also seen in sub-mm CO studies, e.g., Cernicharo et al. 1989; Young et al. (1992); and in the CS J=2-1 by Haijan et al. (1995), indicating that shock heating may also play an important role.

Latter et al. (1992) successfully modelled the observed H_2 emission using a fluorescence model. A more recent study also showed evidence of shock from H_2 emission lines (Hora & Latter 1999). From the KAO results (Justtanont et al. 1997), it was suggested that the main heating source is due to the FUV field from the hot central star. Here, we compare the LWS observations with a grid of C-rich PDR models and the best fit models indicate, again, a high density of 10^7 cm^{-3} and a high G_0 of 10^7 (Fig. 7). The density and the radiation field are high because the object is very compact ($\Omega \sim 2 \cdot 10^{-10}$ sr). Such high values of n and G_0 are consistent with the presence of much higher-J CO lines than in the spectra of AFGL 2688 and NGC 7027. The observations seem to lie just above the models, which may indicate that the source size used here is too small.

Since a fast wind has been observed in AFGL 618, we also consider the effect of shock heating. If we compare the observed CO line intensities, assuming the above source size, we can reasonably fit them with the model from HM89 with $n_0 = 10^6 \text{ cm}^{-3}$ and $v_s = 150 \text{ km s}^{-1}$, by scaling the intensities of lines up by the CO abundance assumed here, i.e., $6.2 \cdot 10^{-4}$. The low velocity shock models predict CO line intensities an order of magnitude below the observations (Fig. 7). Hence the heating mechanism in this object can be explained by either a PDR or high velocity shock since the morphology of the object is very complicated. Here, we have assumed that the H_2 and CO emission arises from the same region, which may not necessarily be the case.

The atomic fine structure lines of [O I] 63 μm and [C II] 158 μm are also seen in the LWS spectrum. The [O I] 146 μm line may be blended with the much stronger CO J=18-17 line (Fig. 1). The [O I] and [C II] lines could indicate a PDR or a shock. If they originate in a shock, the [O I]/[C II] ratio should be relatively high due to the weakness of the [C II] 158 μm line. The [O I] 63 μm line was observed with the LWS in its Fabry-Perot mode (PI: M. Meixner) which has a resolution of 8 000. The profile, although it has a relatively low signal-to-noise and is resolved and does not show the broadening of 200 km s^{-1} seen in the sub-mm data (Fong, 1999 Priv. comm). In order to explain the observed CO line with shocks, we need a shock velocity of $\geq 150 \text{ km s}^{-1}$. Hence, we conclude that the most likely heating source for the gas is a PDR.

6.3. NGC 7027

This is one of the best studied planetary nebulae. It has a very hot central star with a temperature of $\sim 2 \cdot 10^5 \text{ K}$ (Latter et al. 2000). At such a high temperature, the star also produces soft X-rays. The line profiles of molecular H_2 show no evidence for a fast wind in the system (Cox et al. 1997), therefore it is most likely that the heating of the gas is dominated by FUV photons from the central star. The nebula is C-rich, with an estimated C/O ratio of 3 (Shields 1978).

From the IR images of NGC 7027 by Graham et al. (1993) and by Cox et al. (1997), we assume that the CO emission originates from the dense torus of $2'' \times 9''$, i.e., the source size (Ω) is $4 \cdot 10^{-10} \text{ sr}$. The best fit PDR model gives a density of 10^6 cm^{-3} and a radiation field of $\leq 10^7$ times the interstellar value (Fig. 8). The more recent HST/NICMOS images of NGC 7027 reveal a very complex structure with one, or possibly two, bipolar outflows (Latter et al. 2000). Yan et al. (1999) calculated a thermal and chemical model for NGC 7027. Their model was able to reproduce observed line fluxes from LWS spectra quite well. However, we find significant differences in their calculated temperature and those of our PDR models. In our models, the gas temperature remains high from the surface ($\sim 4\,000 - 6\,000 \text{ K}$) and drops sharply at $A_v \gtrsim 1$ to $\sim 100 \text{ K}$.

We also compare the expected fluxes for the atomic fine structure lines which provide major cooling for the envelope. The observed LWS fluxes of the [O I] 63 μm and 146 μm lines are $5.7 \cdot 10^{-17}$ and $2.1 \cdot 10^{-18} \text{ W cm}^{-2}$, respectively, and for the [C II] 158 μm line is $4.0 \cdot 10^{-18} \text{ W cm}^{-2}$. Both the [O I] 63 μm and [C II] 158 μm line fluxes are in reasonably good agreement with the earlier observations by Dinerstein et al. (1991). From the fluxes of the [O I] 63 μm and [C II] 158 μm lines, the observed [O I]/[C II] ratio is in line with those observed for other PDRs (Hollenbach & Tielens 1997) and PDR models (Kaufman et al. 1999; Wolfire et al. 1990). However, the PDR models fail to reproduce the observed absolute intensities of these lines. This points towards the source size for which these fine structure lines arise from being much larger, i.e. $> 10^{-9} \text{ sr}$. This larger size corresponds to the halo seen in the H_2 image surrounding the denser torus (Graham et al. 1993; Latter et al. 2000). The density in the halo is also expected to be less than the smaller

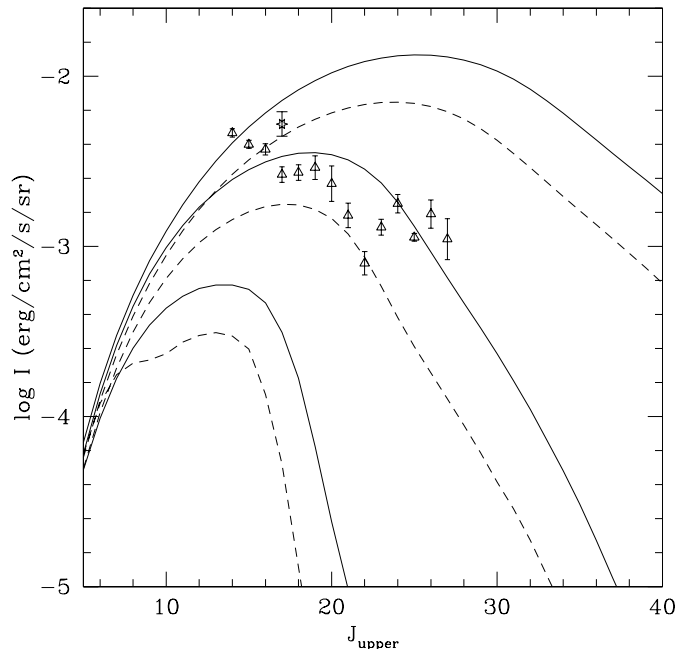


Fig. 8. Comparison between the LWS (triangles) and KAO (star) CO line intensities for NGC 7027 and the PDR models (see Fig. 5 for keys to the lines). The assumed source size is $4 \cdot 10^{-10} \text{ sr}$.

torus region. We are able to reasonably fit the observed [O I] and [C II] line fluxes with a model with $n = 10^5 \text{ cm}^{-3}$ and $G_0 = 10^7$, assuming a source size of $5 \cdot 10^{-9} \text{ sr}$. A similar conclusion was reached by Burton et al. (1990) and Justtanont et al. (1997).

Natta & Hollenbach (1998) calculated the effect of soft X-rays on the neutral gas in a time-dependent PDR and showed that this mainly affects H_2 chemistry as well as atomic and ionized species. We also investigated the effect of X-ray photons on the heating of the gas. As expected, X-rays only affect the surface of the PDR where the visual extinction is low ($A_v \leq 0.1$). This thin layer does not contribute substantially to the CO, [O I] and [C II] lines. Beyond this point, these soft X-rays can no longer penetrate the PDR, hence the temperature remains unchanged.

7. Summary

We have investigated the ISO-LWS spectra of three C-rich objects in differing evolutionary stages after leaving the AGB. All show highly excited CO rotational lines which imply warm dense gas. Assuming the lines are optically thin, we estimate the rotation temperatures of 350-700 K and masses of $0.1 M_\odot$. From optically thin slab calculations, taking into account the excitation, we derive a density of $\sim 10^6 - 5 \cdot 10^7 \text{ cm}^{-3}$. Alternatively, high temperature and low density models can also fit the data. We considered two different mechanisms to explain the observed lines: PDRs and shocks. In this way, we can specify the density via the calculation of heating and cooling of the gas. We presented grids of models for C-rich chemistry PDRs and for shocks. The former fully take into account the C-rich

chemistry. We assumed C/O = 3 by number for the PDR models (Shields 1978).

For the least evolved object in our sample, AFGL 2688, the gas is most likely to be heated by low velocity ($\sim 20 \text{ km s}^{-1}$) shocks. This model can also explain the lack of detection of the atomic fine structure lines of [O I] and [C II] since a 20 km s^{-1} shock is not strong enough to ionize carbon or dissociate much of CO into atomic oxygen. The required preshock density for the best fit shock model is $n_0 \lesssim 10^6 \text{ cm}^{-3}$. Note that the CO emission comes from higher density postshock gas therefore the derived density from the LTE, optically thin slab reflects the high postshock density.

The intermediate case of AFGL 618 can be explained by either FUV-heating ($T_{\text{eff}} \sim 3 \cdot 10^4 \text{ K}$), or by high-velocity shock heating. Both models, again, require a preshock density of 10^7 cm^{-3} . LWS-FP observations of the [O I] $63 \mu\text{m}$ line do not show evidence for the fast wind of 200 km s^{-1} seen in the sub-mm data. Hence we conclude that the main heating source in this object is most likely a PDR.

For NGC 7027, the spectrum is compatible with FUV heating in a PDR. The required density is 10^6 cm^{-3} with a radiation field, $G_0 \lesssim 10^7$ times the interstellar value. Our models indicate that heating due to X-rays has little effect on the CO line fluxes. The [O I] and [C II] atomic fine structure line fluxes imply the presence of a large halo of lower density, somewhat cooler gas.

Acknowledgements. W.B.L. and A.G.G.M.T. acknowledge support from NASA grant 399-20-61 from the Long Term Space Astrophysics Program. We thank the referee, Dr. Tsuji for his comments which resulted in an improvement of the discussion of this paper.

References

- Bakes E.L.O., Tielens A.G.G.M., 1994, ApJ 427, 822
 Burton M.G., Hollenbach D.J., Tielens A.G.G.M., 1990, ApJ 365, 620
 Cernicharo J., Barlow M.J., González-Alfonso E., et al., 1996, A&A 315, L201
 Cernicharo J., Guélin M., Martín-Pintado J., Penalver J., Mauersberger R., 1989, A&A 222, L1
 Clegg P., Ade P.A.R., Armand C., 1996, A&A 315, L38
 Cohen M., Hollenbach D.J., Haas M.R., Erickson E.F., 1988, ApJ 329, 863
 Cox P., González-Alfonso E., Barlow M.J., et al., 1996, A&A 315, L265
 Cox P., Maillard J.-P., Huggins P.J., et al., 1997, A&A 321, 907
 Cox P., Lucas R., Huggins P.J., et al., 2000, A&A 353, L25
 Crampton D., Cowley A.P., Humphreys R.M., 1975, ApJ 198, L135
 de Jong T., Chu S.-I., Dalgarno A., 1975, ApJ 199, 69
 Dinerstein H.L., Haas M.R., Werner M.W., 1991, BAAS 23, 915
 Draine B.T., McKee C.F., 1993, ARA&A 31, 373
 Graham J.R., Serabyn E., Herbst T.M., et al., 1993, AJ 105, 250
 Habing H.J., 1968, Bull. Astr. Inst. Netherlands 19, 421
 Haijan A.R., Phillips J.A., Terzian Y., 1995, ApJ 446, 244
 Hollenbach D.J., McKee C.F., 1989, ApJ 342, 306 (HM89)
 Hollenbach D.J., Tielens A.G.G.M., 1997, ARA&A 35, 179
 Hora J.L., Latter W.B., 1994, ApJ 437, 281
 Hora J.L., Latter W.B., Deutsch L., 1999, ApJS 124, 195
 Justtanont K., Skinner C.J., Tielens A.G.G.M., Meixner M., Baas F., 1996, ApJ 456, 337
 Justtanont K., Tielens A.G.G.M., Skinner C.J., Haas, M.R., 1997, ApJ 476, 193
 Kaufman M.J., Wolfire M.G., Hollenbach D.J., Luhman M.L., 1999, ApJ 527, 795
 Kessler M.F., Steinz J.A., Anderegg M.E., et al., 1996, A&A 315, L27
 Latter W.B., Maloney P.R., Kelly D.M., et al., 1992, ApJ 389, 347
 Latter W.B., Hora D.M., Kelly D.M., et al., 1993, AJ 106, 260
 Latter W.B., Dayal A., Biegging J.H., et al., 2000, ApJ, in press
 Lester D.F., Werner M.W., Storey J.W.V., Watson D.M., Townes C.H., 1981, ApJ 248, L109
 Liu X.-W., Barlow M.J., Rieu N.-Q., et al., 1996, A&A 315, L257
 Liu X.-W., Barlow M.J., Dalgarno A., et al., 1997, MNRAS 290, L71
 McKee C.F., Storey J.W.V., Watson D.M., Green S., 1982, ApJ 259, 647
 Maun N., Huggins P.J., 1999, A&A 349, 203
 Natta A., Hollenbach D., 1998, A&A 337, 517
 Pottasch S.R., 1996, A&A 307, 561
 Sahai R., Hines D.C., Kastner J.H., et al., 1998a, ApJ 492, 163
 Sahai R., Trauger J.T., Watson A.M., et al., 1998b, ApJ 493, 301
 Schmidt G.D., Cohen M., 1981, ApJ 246, 444
 Shields G.A., 1978, ApJ 219, 565
 Skinner C.J., Meixner M., Barlow M.J., et al., 1997, A&A 328, 290
 Spaans M., Tielens A.G.G.M., van Dishoeck E.F., Bakes E.L.O., 1994, ApJ 437, 270
 Swinyard B.M., Clegg P.E., Ade P.A.R., et al., 1996, A&A 315, L43
 Tielens A.G.G.M., Hollenbach D.J., 1985, ApJ 291, 722 (TH85)
 Wolfire M.G., Tielens A.G.G.M., Hollenbach D.J., 1990, ApJ 358, 116
 Yan M., Federman S.R., Dalgarno A., Bjorkman J.E., 1999, ApJ 515, 640
 Young K., Serabyn S., Phillips T.G., et al., 1992, ApJ 385, 265